Flame dynamics in oscillating flows under autoignitive conditions

Sili Deng[a,*], Peng Zhao[a,b], Michael E. Mueller[a], Chung K. Law[a]

[a] *Department of Mechanical and Aerospace Engineering, Princeton University, Princeton, NJ 08544, USA*
[b] *Department of Mechanical Engineering, Oakland University, Rochester, MI 48309, USA*

Abstract

The structure and dynamics of laminar nonpremixed dimethyl ether (DME)/air coflow flames were investigated at elevated temperatures and pressures. Computations with detailed chemistry were performed for DME and heated coflow air at 30 atm with uniform but sinusoidal oscillating inlet velocities. These unsteady cases were compared with the steady results from Deng *et al.* (Combust. Flame in press) to elucidate oscillation frequency effects on flame dynamics. A normalized displacement velocity was defined to differentiate flame propagation from autoignition, and this definition was validated against the steady cases to benchmark the unsteady cases. In the oscillating reacting flow, transition between a multibrachial autoignition front and a tribrachial flame occurs periodically. However, unlike the harmonic velocity oscillation, the combustion mode transition is hysteretic. As flow velocity decreases, the upstream of the autoignition front does not have sufficient time to respond, and therefore autoignition chemistry remains the dominant chemical pathway. Near the lower velocity limit, due to the slower velocity change, the chemical state of the upstream unburnt mixture relaxes closer to steady state, and flame chemistry becomes dominant. As flow velocity increases again, the tribrachial flame is convected downstream, and heat and radical back diffusion from the flame becomes less important, such that the upstream mixture remains unburnt. Due to the radical and heat accumulation, autoignition eventually occurs and becomes the dominant pathway. The finite induction time for autoignition results in the hysteretic behavior of the upstream-traveling and downstream-traveling processes, which diminishes at lower oscillation frequency, as there is more time for chemistry to respond to hydrodynamic changes and approach steady state.

Keywords: Flame dynamics, Nonpremixed coflow flame, Autoignition, Negative temperature coefficient (NTC), Dimethyl ether (DME)

[*] Corresponding Author: silideng@princeton.edu

1. Introduction

To facilitate well-controlled and highly-efficient combustion processes, practical internal combustion engines often operate under nonpremixed, elevated temperature and pressure, and turbulent conditions. Due to experimental and computational limitations, however, simplifications are usually made to obtain fundamental understanding of these complex reacting flows. For example, laminar nonpremixed coflow flames at normal ambient temperatures are studied to elucidate the coupling between fluid dynamics and chemistry. In the fuel and oxidizer mixing layer, a two-dimensional tribrachial structure (also known as triple flame) [1] is observed. Specifically, both lean and rich premixed flame branches and a trailing diffusion flame tail intersect at a triple point. Based on the observation of such tribrachial flame, the partially premixed flamelet model [2] was proposed to explain lifted flames in nonpremixed turbulent jets [3].

To bridge the gap between laminar and turbulent combustion, unsteady nonpremixed coflow flames are studied. It is found that pollutant formation, such as soot [4, 5] and carbon monoxide [6], is more pronounced in unsteady reacting flows. Moreover, flame structure and propagation can be influenced by the unsteadiness as well. As reviewed by Chung [3], the propagation speed of tribrachial flame is affected by thermal expansion [7], mixture fraction gradient [8], and flame curvature [9], where the unsteady curvature term plays a dominant role [10]. To demonstrate the unsteady interactions between flow and flame, Strawa and Cantwell [11] imposed a small-amplitude, periodic velocity fluctuation to nonpremixed jet flames at elevated pressures and low Reynolds numbers. In their experiments, periodic eddy formation and flame breakup was achieved by varying the excitation frequency. Dworkin *et al.* [12] conducted computational and experimental study of a periodically-forced methane/air coflow diffusion flame and found that the oxidation of CO to CO_2 was inhibited in unsteady flows. 30% and 50% sinusoidal velocity perturbations were imposed on the fuel jet at a fixed frequency of 20 Hz, and CO and H_2O mole fraction profiles were compared to verify their model and describe the dynamics of the flame. It was found computationally by Sánchez-Sanz *et al.* [13] that flame thermal and chemical properties in such periodically time-varying flows were affected by the imposed perturbation frequency. Three regimes were found depending on the flame's Strouhal number, $S = af/U$, with a and f denoting the fuel jet radius and perturbation frequency, respectively. For small Strouhal number ($S = 0.1$), perturbation can travel far downstream, resulting in an oscillating flame. A flickering flame was observed when $S \simeq 0.2$, and a vigorous flame pinch-off was observed at $S = 0.5$. Larger values of S confine the oscillation to the jet's near-exit region, and the pulsation has minimal effects on temperature and concentration values.

Although demonstrating the unsteady effects on flow-chemistry coupling, these experimental and computational investigations mainly focused on simple fuels, such as methane, and were limited to nonautoignitive conditions. Taking more complex chemical kinetics and elevated temperature and pressure engine conditions into account, Krisman *et al.* [14] first computationally demonstrated that besides the traditional tribrachial flame, autoignition is also a relevant combustion process, or even the dominant one under certain conditions. Their findings were confirmed and further discussed by Deng *et al.* [15, 16] recently through a series of computational studies of nonpremixed dimethyl ether (DME)/air coflow flames at 30 atm with varying inlet velocities and coflow temperatures. One-dimensional Lagrangian Flamelet Analysis (LFA) was compared with two-dimensional computation to differentiate the combustion modes. A regime diagram was proposed to demonstrate that the tribrachial flame is favored at lower inlet velocity and higher coflow temperature, while autoignition is dominant at higher inlet velocity and relatively lower coflow temperature.

In the present study, unsteady nonpremixed coflow flames under autoignitive conditions are computationally studied to elucidate the coupling between fluid dynamics and chemical kinetics. Various oscillation frequencies were imposed on the inlet velocity, with the maximum and minimum velocities maintained the same as those in the previous steady study [16], which corresponds to a tribrachial flame and an autoignition front, respectively. The objective of the current study is threefold. First, to capture the transition in combustion mode. As the steady cases correspond to different combustion modes, it is expected that at certain frequencies of velocity oscillation, the dominant combustion process will shift between nonpremixed flame and autoignition. Second, to assess the thermal and chemical differences during such transition and to elucidate the transition mechanism. And third, to demonstrate the oscillation frequency effects on the coupling of fluid dynamics and chemical kinetics.

2. Computational details

Axisymmetric coflow flames under 30 atmospheres were computed, where a 300 K DME stream is sur-

rounded by 900 K air stream. The diameter (D) of the fuel nozzle is 0.8 mm, which is 20 times the thickness of the adiabatic, no-slip wall, separating fuel and coflow. The coflow outer diameter is 3.9 mm, with adiabatic, slip wall conditions. The same inlet velocities were imposed for both streams and are uniform in space and sinusoidally oscillating in time. The maximum (8.0 m/s) and minimum (2.4 m/s) velocities were set to match the fastest and slowest steady cases as in Deng *et al.* [16]. Three oscillation frequencies (25, 50, and 100 Hz) was investigated, with the maximum Strouhal number estimated based on the jet radius $D/2$ is smaller than 0.02 to avoid flame pinch-off. The domain length is 15 mm, with a convective outflow boundary condition. The computational results were not affected by further broadening or lengthening of the domain. Discretization of the domain was guided by the grid convergence studies [15], with a 3072 (x) by 176 (r) grid. Uniform spacing in the axial direction was set to $\Delta x = 4.8$ μm, and nonuniform spacing in the radial direction was set to minimum $\Delta r = 2.5$ μm to resolve the mixing layer near the thin wall. The grid stretch rate is less than 3%.

The Navier-Stokes equation with buoyancy effects in the streamwise direction and the conservation equations of mass, species, and energy were solved. The species diffusivities were determined assuming a constant, nonunity Lewis number and kept the same as in Deng *et al.* [15]. The conserved scalar, mixture fraction (Z), was specified as unity and zero for the fuel stream and coflow, respectively, and was computed by solving a conserved scalar transport equation with unity Lewis number [17]. DME was chosen as the fuel, for it is one of the simplest fuels that have the Negative Temperature Coefficient (NTC) chemistry [18], which is highly relevant to engine knock [19]. A skeletal mechanism of 39 species [20], which was reduced from the well-validated detailed mechanism of Zhao *et al.* [21], was adopted as the chemical model.

A low-Mach number code NGA [22] was adopted to solve the discretized governing equations on a staggered mesh. A second-order centered scheme was used for the momentum equations, while a third-order WENO scheme [23] was used for the scalar equations. An iterative second-order semi-implicit Crank-Nicolson scheme was adopted for temporal integration [24]. The chemical source terms for the species and energy equations were integrated using the CVODE package [25].

3. Results and discussion

As the largest and smallest inlet velocity cases were designed to match the two extreme cases in Deng *et al.* [16], which are of different thermal structures, it is expected that similar thermal structures will be obtained. Furthermore, these thermal structures might transition back and forth due to the oscillating flow field. Indeed, such transitions were observed for all three frequencies. For example, the evolution of the thermal structure of the 100 Hz case, in terms of the heat release rate profile, is demonstrated in Fig. 1. The oscillation cycle starts with the largest inlet velocity of 8.0 m/s, and the minimum inlet velocity (2.4 m/s) is achieved at half cycle.

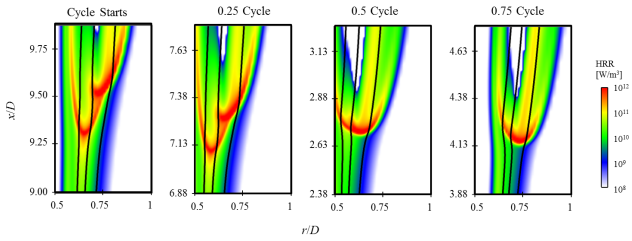

Figure 1: Heat release rate [W/m^3] profile evolution during one oscillation cycle at 100 Hz. The iso-contours of $Z_{st} = 0.1$, $Z = 0.2$, and $Z = 0.3$ are outlined from right to left in solid lines, respectively.

At 8.0 m/s, the multibrachial thermal structure is located furthest downstream. The leading point, which is defined as the most upstream point that has the heat release rate value of 10^{12} W/m^3, is located at mixture fraction $Z = 0.24$. As inlet velocity decreases, the multibrachial structure moves upstream, without obvious change of the leading point location, in terms of mixture fraction. When the inlet velocity reaches minimum, the multibrachial structure transitions to a tribrachial structure, and the leading point switches to $Z = 0.14$. As flow velocity increases, the tribrachial structure is pushed downstream. However, its tribrachial shape as well as the leading point mixture fraction remains unchanged. The thermal structure returns to multibrachial, when the flow velocity further increases. Such transitions in structure repeat, as a new oscillation cycle starts.

As mentioned in the Introduction, Deng *et al.* [16] were able to relate the morphology of the thermal structures to two different combustion modes: tribrachial flame and autoignition. In their study, species mass fraction profiles at the inlet of the two-dimensional computation were treated as the initial conditions for one-dimensional Lagrangian Flamelet Analysis [26], which only considers diffusion processes parallel to mixture fraction gradient and neglects the normal direction. When the LFA prediction agrees with the CFD result, transport in the normal direction of the mixture fraction gradient is negligible, and autoignition is the dominant

combustion process. Specifically, at steady state, the multibrachial structure in the 8.0 m/s case is an autoignition front, while the 2.4 m/s case is a tribrachial flame. However, due to the unsteadiness in the current study, such comparison between LFA and CFD is not valid anymore. Therefore, a new criterion to differentiate tribrachial flame and autoignition needs to be derived and validated against the steady cases.

A density-weighted displacement speed, S_d, is often used to distinguish between deflagrations and spontaneous ignition fronts in HCCI combustion [27], which is defined from an iso-line of species k as [8, 28]:

$$S_d = \frac{1}{\rho_u |\nabla Y_k|} \left(\dot{\omega}_k - \frac{\partial \rho Y_k V_{j,k}}{\partial x_j} \right), \qquad (1)$$

where Y_k, $V_{j,k}$, and $\dot{\omega}_k$ denote species mass fraction, diffusion velocity in the j-direction, and net production rate, respectively, and ρ_u is the density of the unburnt mixture. The choice of species k and its iso-line value can be ambiguous. Therefore, major products, such as CO_2, H_2O, H_2, CO, and combinations of these products have been tested, and the sampling location is chosen as the leading point to enable further comparison with the steady cases. S_d at the leading point is insensitive to the choice of species in the current study, for less than 5% difference was observed across all the combinations. For simplicity, H_2O was chosen. In order to compare this displacement velocity with the corresponding laminar flame speed S_L, the unburnt mixture density ρ_u was obtained from the laminar flame speed calculation using the FlameMaster code [29]. The composition boundary conditions for the laminar flame speed calculation was estimated from the mixture fraction at the leading point, and the temperature boundary condition was estimated assuming pure mixing of fuel and heated air with their inlet values in the two-dimensional computation.

Following the above procedure, displacement velocities were calculated for all three oscillation frequency cases, with 20 points per cycle to demonstrate their evolution. Furthermore, as shown in Fig. 2, S_d/S_L for the two steady cases (2.4 and 8.0 m/s) were similarly calculated to validate this definition of normalized displacement velocity and benchmark tribrachial flame and autoignition.

The normalized displacement velocities for the steady autoignition front and tribrachial flame are denoted in Fig. 2 as the top and bottom horizontal lines, respectively. The S_d/S_L for the steady tribrachial flame is around unity, while for the autoignition front this value is around eight. These values are similar to those in HCCI combustion studies [27] and therefore can be

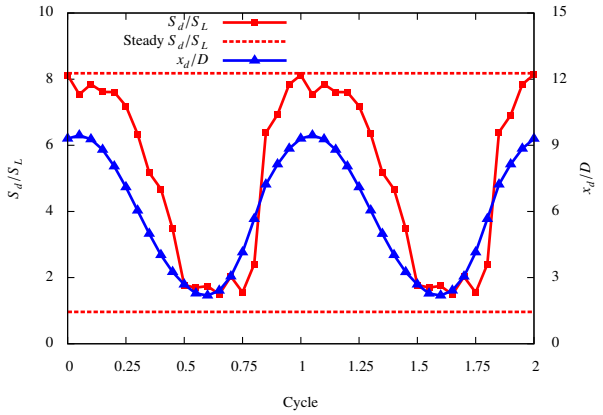

Figure 2: Normalized displacement velocity (red) and location (blue) time history profiles at 100 Hz. The other two frequency cases show qualitatively the same evolution and are therefore not shown for clarity.

used to benchmark the unsteady cases. The periodic time history profile of S_d/S_L is bounded by but has not fully reached the two steady values, indicating that fluid dynamics and chemical kinetics are coupled and their time scales are comparable. It is noted that S_d/S_L almost remains constant, when its value approaches the tribrachial flame limit, while the change near the autoignition limit is more sinusoidal. Moreover, since 20 points were sampled evenly in time, S_d/S_L changes more abruptly when the combustion mode switches from tribrachial flame to autoignition. Compared to the normalized leading point location (x_d/D) profile, which is almost sinusoidal, the normalized displacement velocity profile is asymmetric, indicating that the transition from tribrachial flame to autoignition as the inlet velocity increases is not an exact reverse process of the transition from autoignition to tribrachial flame. Indeed, as shown in Fig. 1, although the inlet velocities at 0.25 and 0.75 cycle are the same, the upstream/downstream-traveling structures have different morphology: there is hysteresis during the transition.

Such hysteresis is demonstrated more clearly in Fig. 3, where S_d/S_L is plotted against the inlet velocity. Qualitatively, all three oscillation frequency cases show similar trends: given the same inlet velocity, hence boundary condition, upstream/downstream-traveling structures have different displacement velocities. Moreover, from the heat release rate profile history (partially included in Fig. 1), it is seen that the leading point locates around $Z = 0.24$ moving upstream, while its location shifts to leaner mixture fraction $Z = 0.14$ when the inlet velocity reaches minimum, and the lead-

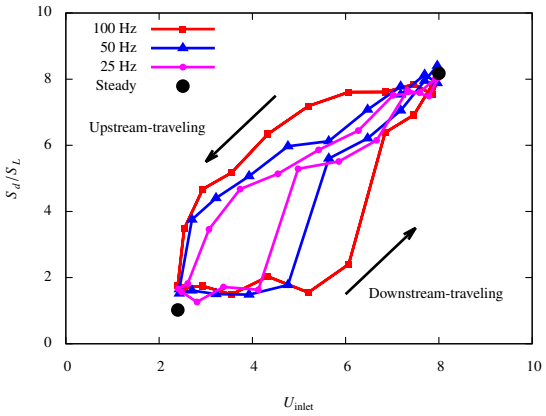

Figure 3: Normalized displacement velocities at various inlet velocities, for two steady cases and three oscillating unsteady cases.

ing point location shifts back to $Z = 0.24$, when U_{inlet} exceeds 6.4 m/s. The shift in leading point mixture fraction as well as displacement velocity indicates different dominant chemical reactions.

In the steady case analysis [16], the dominant chemical pathways are different at the leading point of the tribrachial flame and autoignition front. Specifically, the hydrogen peroxide branching reaction ($H_2O_2 + M \Longleftrightarrow OH + OH + M$) is the dominant chain branching reaction at the leading point of the autoignition front, while the H radical branching reaction ($H + O_2 \Longleftrightarrow O + OH$) is the most important chain branching reaction at tribrachial flame leading point. Due to longer residence time, hydrogen peroxide accumulation is much higher upstream of the autoignition front compared to the tribrachial flame front. As hydrogen peroxide plays different roles in tribrachial flame and autoignition front, its spatial profiles along the $Z = 0.24$ iso-contour are compared in Fig. 4, with the left and right subfigures corresponding to the upstream-traveling and downstream-traveling half cycles, respectively.

The left figure shows that hydrogen peroxide keeps on accumulating until either autoignition happens or it is consumed at the flame front, and its mass fraction sharply drops. However, the peak value of hydrogen peroxide mass fraction differs by five times between a steady autoignition front and tribrachial flame, which implies its different significance in these two combustion modes and sets the benchmark for the unsteady evolution. As the inlet velocity decreases from 8.0 m/s, the peak $Y_{H_2O_2}$ almost remains constant and is very close to the steady autoignition case. As flow velocity decreases, a larger gradient is achieved, resulting in steeper profiles, and hence, lower S_d/S_L, according to Eq. (1). The

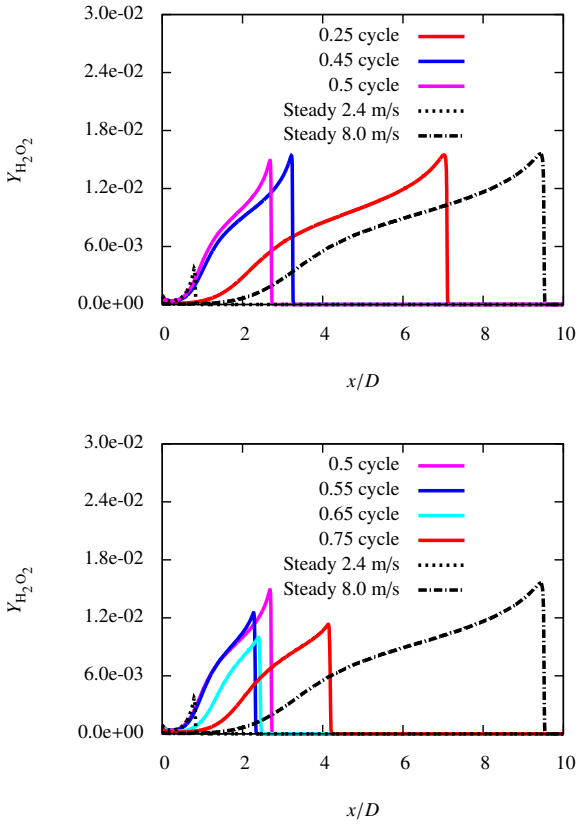

Figure 4: The comparison of hydrogen peroxide mass fraction profile along $Z = 0.24$ iso-contour at steady state and at 100 Hz during upstream-traveling cycle (left) and downstream-traveling cycle (right).

upstream chemical structure barely deviates from the steady autoignition case. As a consequence, the dominant chemical pathway remains to be H_2O_2 + M $\Longleftrightarrow$ OH + OH + M, and autoignition is the dominant combustion process, resulting in high S_d/S_L.

Even when the inlet velocity reaches 2.4 m/s at 0.5 cycle, which is the same as the steady case, the reacting front still moves upstream, which is also shown in Fig. 2. Inlet velocity changes slowest around the half cycle, when the chemical structure starts to respond. As shown on the right of Fig. 4, the peak $Y_{H_2O_2}$ decreases from 0.5 to 0.65 cycle. At this stage, autoignition is not fully activated, however, hydrogen peroxide accumulation is still stronger than a steady tribrachial flame. Therefore, the S_d/S_L of the tribrachial structure is close to but slightly higher than a steady flame, as it is propagating into a partially reacting mixture. This tribrachial structure is convected downstream, as inlet velocity further increases from 0.65 to 0.75 cycle. Flame back diffusion becomes less important due to stronger convection and shallower species profiles. The unburnt mixture upstream of the flame accumulates radicals and heat, as it moves downstream. It finally autoignites, denoted by a sudden jump of S_d/S_L.

The other two lower oscillation frequency cases are similar qualitatively, but with some quantitative differences. As shown in Fig. 3, upstream/downstream-traveling hysteresis is diminished as the oscillation frequency decreases, denoted by the shrink of the enclosed area. Hysteresis remains at slower inlet velocities, since the upstream-traveling branch is still autoignition dominant, while it takes finite induction time for the downstream-traveling unburnt mixture to achieve autoignition. At higher inlet velocities, both branches are autoignition dominant and therefore collapse to a single path at sufficiently low frequency, approaching the quasi-steady state limit.

Interestingly, although relatively the 100 Hz case demonstrates hysteresis for a larger portion of its oscillation cycle, in terms of the absolute time, it takes the 25 Hz case longer time to achieve the transition from low S_d/S_L to higher values, indicating a longer induction time. This counter-intuitive finding is explained with Fig. 5. Hydrogen peroxide profiles are compared among three frequency cases for both upstream and downstream-traveling branches, at the same inlet velocity of 3.2 m/s, and benchmarked with the corresponding steady computation. According to previous studies [15, 16], this steady case is autoignition dominant at Z = 0.24. Three unsteady profiles on the upstream-traveling branch show similar peak values, and, the lower the frequency, the closer the profile matches the

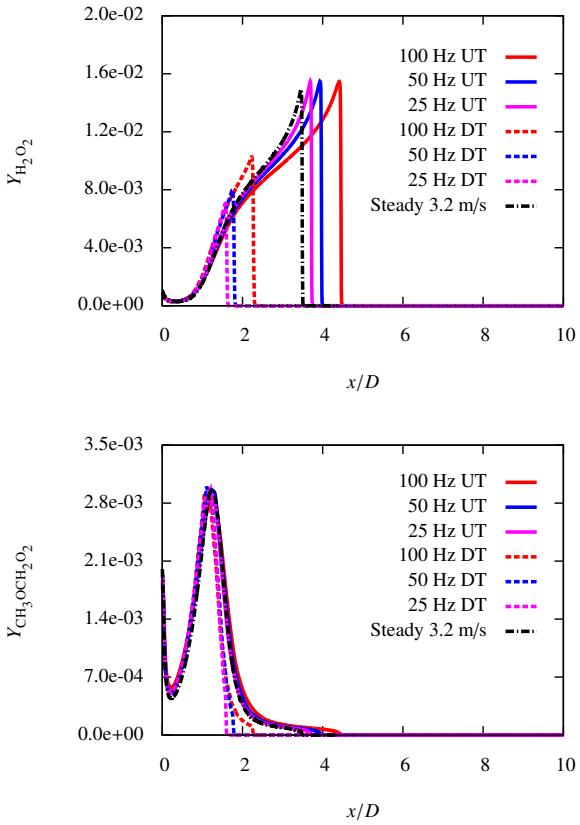

Figure 5: Hydrogen peroxide and methyoxymethylperoxy radical mass fraction profiles along Z = 0.24 iso-contour at 3.2 m/s. UT: upstream-traveling, and DT: downstream-traveling.

steady case, which is expected. However, the unsteady profiles on the downstream-traveling branch show lower peak values. Moreover, the 100 Hz case profile is closer to the steady counterpart. Noting from Fig. 3 that the minimum S_d/S_L in all three cases are higher than the steady 2.4 m/s case and at lower frequency the unburnt mixture has longer time to relax to steady state, the 25 Hz case should match the 2.4 m/s steady case closer. Therefore, it takes this case longer time to accumulate sufficient hydrogen peroxide to activate autoignition. Conversely, the 100 Hz case allows less time to relax to a steady flame structure and therefore has higher $Y_{H_2O_2}$ to start with the downstream-traveling cycle, resulting in a shorter induction time for autoignition.

As demonstrated in previous studies [15, 16], NTC chemistry is important in the upstream of both tribrachial flame and autoignition front. The methoxymethylperoxy radical ($CH_3OCH_2O_2$) is chosen to represent NTC chemistry [14], and $Y_{CH_3OCH_2O_2}$ profiles are shown in Fig. 5 to elucidate oscillation fre-

quency effects on NTC chemistry. It is seen that irrespective of the oscillation frequency and traveling direction, at the same inlet velocity, $Y_{CH_3OCH_2O_2}$ matches with its steady state profile. Comparing with the distinct behavior of $Y_{H_2O_2}$, it is seen that the NTC chemistry time scale is relatively short compared to the accumulation of hydrogen peroxide. The induction time for the first-stage ignition facilitated by NTC chemistry is relatively short ($\sim$ 0.3 ms [16]), compared to the major autoignition process induced by hydrogen peroxide branching reaction ($\sim$ 1 ms [16]) and the characteristic hydrodynamic oscillation time (10-40 ms in the current work). Therefore, NTC chemistry can be decoupled from flow dynamics. Conversely, the coupling between fluid dynamics and second-stage autoignition/flame is important.

4. Conclusions

Axisymmetric laminar nonpremixed DME coflow flames at elevated temperatures and pressures with sinusoidally oscillating inlet velocities were computationally investigated. The inlet velocity oscillates between 2.4 and 8.0 m/s, at 25, 50, and 100 Hz. Flame dynamics in such oscillating flows and frequency effects on the hydrodynamics-chemistry coupling were elucidated.

The heat release rate profiles were examined to describe the thermal structure. The morphology of the thermal structure transitions between tribrachial and multibrachial. Multibrachial structure is favored when inlet velocity is higher, although there is hysteresis during the transition. Such structures agree well with the steady cases in Deng *et al.* [16], which correspond to different combustion modes: tribrachial flame and autoignition. Normalized displacement velocity was defined to differentiate these two modes in the current study and compared with the steady cases.

According to the steady results, the normalized displacement velocity for a tribrachial flame is around unity, while for autoignition is higher. The same criterion was applied to the unsteady cases to elucidate the evolution of combustion mode. As the inlet velocity decreases, autoignition is the dominant combustion process until flame chemistry takes over around the most upstream location and slowest inlet velocity. The tribrachial flame is convected downstream as flow velocity increases, and flame back diffusion becomes weaker. The radical and heat accumulation upstream of the tribrachial flame finally results in autoignition, showing a sudden increase of the normalized displacement velocity.

Examining the evolution of methyoxymethylperoxy radical and hydrogen peroxide profiles during the oscillation process, it is found that at the three frequencies investigated, the tribrachial structure does not have sufficient time to reach steady state. Consequently, the upstream-traveling and downstream-traveling cycle have different normalized displacement velocities and hence demonstrate hysteresis. NTC chemistry represented by methyoxymethylperoxy radical accumulation and depletion has shorter time scales and therefore is able to respond to the hydrodynamic changes. However, autoignition and flame establishment have comparable time scales to the oscillation periods, and the lower frequency case is closer to reach steady state condition.

Acknowledgments

This research was supported in part by the Air Force Office of Scientific Research (AFOSR) under the technical management of Dr. Mitat Birkan.

References

[1] J. Buckmaster, Prog. Energy Combust. Sci. 28 (2002) 435–475.
[2] C. M. Müller, H. Breitbach, N. Peters, Proc. Combust. Inst. 25 (1994) 1099–1106.
[3] S. H. Chung, Proc. Combust. Inst. 31 (2007) 877–892.
[4] C. R. Shaddix, J. E. Harrington, K. C. Smyth, Combust. Flame 99 (1994) 723–732.
[5] R. K. Mohammed, M. A. Tanoff, M. D. Smooke, A. M. Schaffer, M. B. Long, Proc. Combust. Inst. 27 (1998) 693–702.
[6] R. R. Skaggs, J. H. Miller, Proc. Combust. Inst. 26 (1996) 1181–1188.
[7] B. J. Lee, S. H. Chung, Combust. Flame 109 (1997) 163–172.
[8] G. R. Ruetsch, L. Vervisch, A. Liñán, Phys. Fluids 7 (1995) 1447.
[9] T. Plessing, P. Terhoeven, N. Peters, M. S. Mansour, Combust. Flame 115 (1998) 335–353.
[10] Y. S. Ko, S. H. Chung, Combust. Flame 118 (1999) 151–163.
[11] A. W. Strawa, B. J. Cantwell, J. Fluid Mech. 200 (1989) 309–336.
[12] S. B. Dworkin, B. C. Connelly, A. M. Schaffer, B. V. Bennett, M. B. Long, M. D. Smooke, M. P. Puccio, B. McAndrews, J. H. Miller, Proc. Combust. Inst. 31 (2007) 971–978.
[13] M. Sánchez-Sanz, B. A. V. Bennett, M. D. Smooke, A. Liñán, Combust. Theory Modell. 14 (2010) 453–478.
[14] A. Krisman, E. R. Hawkes, M. Talei, A. Bhagatwala, J. H. Chen, Proc. Combust. Inst. 35 (2015) 999–1006.
[15] S. Deng, P. Zhao, M. E. Mueller, C. K. Law, Combust. Flame 162 (2015) 3437–3445.
[16] S. Deng, P. Zhao, M. E. Mueller, C. K. Law, Stabilization of laminar nonpremixed DME/air coflow flames at elevated temperatures and pressures, Combust. Flame, (2015) doi:10.1016/j.combustflame.2015.08.019.
[17] H. Pitsch, N. Peters, Combust. Flame 114 (1998) 26–40.
[18] S. Deng, P. Zhao, D. Zhu, C. K. Law, Combust. Flame 161 (2014) 1993–1997.
[19] F. Battin-Leclerc, Prog. Energy Combust. Sci. 34 (2008) 440–498.

[20] A. Bhagatwala, Z. Luo, H. Shen, J. A. Sutton, T. Lu, J. H. Chen, Proc. Combust. Inst. 35 (2015) 1157–1166.
[21] Z. Zhao, M. Chaos, A. Kazakov, F. L. Dryer, Int. J. Chem. Kinet. 40 (2008) 1–18.
[22] O. Desjardins, G. Blanquart, G. Balarac, H. Pitsch, J. Comput. Phys. 227 (2008) 7125–7159.
[23] X. Liu, S. Osher, T. Chan, J. Comput. Phys. 115 (1994) 200–212.
[24] C. D. Pierce, Progress-variable Approach for Large-Eddy Simulation of Turbulent Combustion, Ph.D. thesis, Stanford University, 2001.
[25] S. D. Cohen, A. C. Hindmarsh, P. F. Dubois, Comput. Phys. 10 (1996) 138.
[26] H. Pitsch, M. Chen, N. Peters, Proc. Combust. Inst. 27 (1998) 1057–1064.
[27] C. S. Yoo, Z. Luo, T. Lu, H. Kim, J. H. Chen, Proc. Combust. Inst. 34 (2013) 2985–2993.
[28] H. G. Im, J. H. Chen, Combust. Flame 119 (1999) 436–454.
[29] H. Pitsch, FlameMaster, A C++ computer program for 0D combustion and 1D laminar flame calculations.